



Relating mechanistic fate with spatial positioning for colloid transport in surface heterogeneous porous media

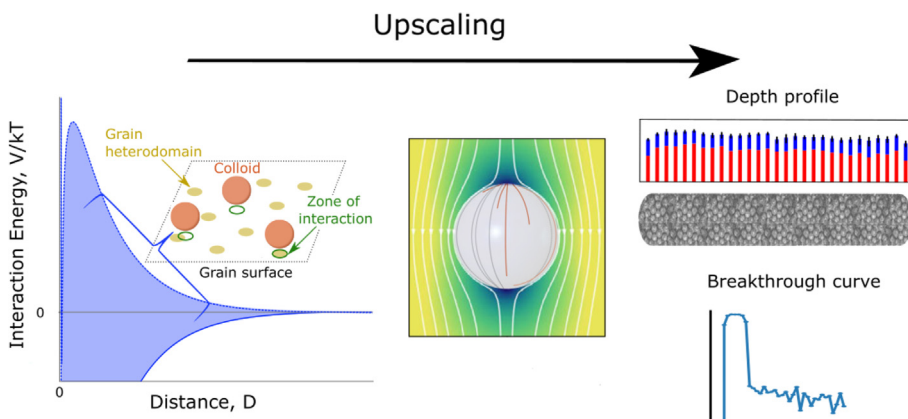


Janis E. Patiño ^a, William P. Johnson ^b, Verónica L. Morales ^{a,*}

^a Department of Civil and Environmental Engineering, University of California at Davis, 1 Shields Ave 2001, Davis 95616, CA, United States

^b Department of Geology & Geophysics, University of Utah, 201 Presidents' Cir, Salt Lake City, 84112, UT, United States

GRAPHICAL ABSTRACT



ARTICLE INFO

Article history:

Received 19 August 2022

Revised 24 February 2023

Accepted 1 March 2023

Available online 9 March 2023

Keywords:

Anomalous transport
interfaces

Surface chemical heterogeneity
X-ray micro-computed tomography

ABSTRACT

Hypotheses: The transport behavior of colloids in subsurface porous media is altered by surface chemical and physical heterogeneities. Understanding the mechanisms involved and distribution outcomes is crucial to assess and control groundwater contamination. The multi-scale processes that broaden residence time distribution for particles in the medium are here succinctly described with an upscaling model.

Experiments/model: The spatial distribution of silver particles along glass bead-packed columns obtained from X-ray micro-computed tomography and a mechanistic upscaling model were used to study colloid retention across interface-, collector-, pore-, and Darcy-scales. Simulated energy profiles considering variable colloid-grain interactions were used to determine collector efficiencies from particle trajectories via full force-torque balance. Rate coefficients were determined from collector efficiencies to parameterize the advective-dispersive-reactive model that reports breakthrough curves and depth profiles. **Findings:** Our results indicate that: (i) with surface heterogeneity, individual colloid-grain interactions are non-unique and span from repulsive to attractive extremes; (ii) experimentally observed spatial positioning of retention at grain-water interfaces and grain-to-grain contacts is governed respectively by mechanistic attachment to the grain surface and retention without contact at rear-flow stagnation zones,

Abbreviations: breakthrough curve, (BTC); chemical heterodomain, (CHD); depth profile, (DP); Derjaguin-Landau-Verwey-Overbeek, (DLVO); grain-to-grain, (GG); Particle Suite, (PS); region of interest, (ROI); rear-flow stagnation zone, (RFSZ); scanning electron microscopy, (SEM); grain-water interface, (GWI); X-ray micro-computed tomography, (μ -CT); zone of interaction, (ZOI).

* Corresponding author.

E-mail addresses: janpatino@ucdavis.edu (J.E. Patiño), william.johnson@utah.edu (W.P. Johnson), vermorales@ucdavis.edu (V.L. Morales).

and (iii) experimentally observed non-monotonic retention profiles and heavy-tailed breakthrough curves can be modeled with explicit implementation of heterogeneity at smaller scales.

© 2023 Elsevier Inc. All rights reserved.

1. Introduction

The transport and fate of colloids (particles of size between 10 nm to 10 μm) suspended in water is a topic of environmental and public health concern. Depending on their origin and composition, their presence in the subsurface can be either viewed as beneficial (e.g. iron oxide nanoparticles used in remediation strategies [1,2]) or detrimental (e.g. viruses, micro- and nano-plastics, and toxic engineered nanomaterials [3–6]). For example, engineered silver colloids used in detergents and anti-odor clothing (due to their biocidal properties [7–9]) have been found in wastewater effluents [10,11] that are subsequently used for irrigation, thus raising concern regarding their impact in groundwater quality and soil microbial communities [12–15]. However, predictions of the distribution of retained colloids in soils, and in environmental porous media in general, are often inaccurate, suggesting a deficient understanding of the processes governing transport and retention in surface heterogeneous systems.

The mass transfer of particles between the liquid and solid phases that govern the filtration of colloids in groundwater systems is a multi-scale problem. Nanoscopic interactions that arise between the surfaces of particles (colloids) and porous media grains dictate how likely colloids will deposit on collector surfaces in hydrodynamic static conditions. When both surfaces are like-charged, a repulsive energy barrier typically hinders deposition (i.e., conditions are so-called *unfavorable*). This situation is commonly observed when studying filtration of environmental colloids [16], since the surfaces of both particles and grains tend to exhibit a net negative charge at typical pH levels in groundwater [17]. Nonetheless, evidence has been repeatedly reported for colloidal retention under *unfavorable* conditions [18–26]. Such observations suggest the presence of at least some *favorable* colloidal interactions along the grain's surface (e.g., as microsites of metal oxides or organic matter), thus questioning the appropriateness of using average system parameters for classic colloid filtration modeling [27]. Using average colloid-grain interactions allows for the straightforward application of classic filtration theory and its variations. However, these do not always correctly capture observations even under simple controlled experimental conditions (e.g. chemically cleaned quartz sand often display non-exponential deposition profiles). Therefore, using average short-range interactions may be responsible for inaccurate predictions of colloid filtration in surface heterogeneous media like natural aquifer environments.

At the smallest of scales, nanoscopic interactions between colloids and grain surfaces are often modeled by Derjaguin-Landau-Verwey-Overbeek (DLVO) theory [28,29], and more recently by extended DLVO, or xDLVO, which considers interactions additional to electric double-layer and van Der Waals (e.g., Born repulsion, Lewis acid-base interactions) [30–32]. A determinant input of these energy calculations is the *average* surface charge of the materials of interest, which is approximated by the measured average ζ -potential. While this approach is commonly used to justify retention trends in porous media, the interactions do not always agree with the amount of retention observed, especially under *unfavorable* conditions [33–36]. Defining system descriptors this way aver-

ages out nano-to-microscale chemical heterogeneities that locally reduce or eliminate repulsion and facilitate deposition. Duffadar et al. [37] point out that all naturally-occurring surfaces are heterogeneous, with great chemical and topographical diversity. In aquifer systems, this leads to the simultaneous existence of favorable and unfavorable interactions between particles in suspension and the filter medium [37,31,25,27,38,39]. Thus, the development of transport models that reflect the stochastic nature of interfacial, and consequently, pore-scale interactions between particles and the granular media has become crucial to improve prediction accuracy of colloid transport in realistically complex porous media [31,25,38–40,6].

The overall transport behavior of colloids in porous media is controlled by colloid-grain interactions that are relevant at separation distances of tens to hundreds of nanometers (interface-scale) [41], flow properties that are relevant at micro- to millimeter distances (pore-scale), and filtration rates determined at centimeter to meter lengths (Darcy-scale). Classic filtration theory assumes deposition to be a two step probabilistic process. The first probability is for intercepting the grain and the second is for attaching to it as η_0 and α , respectively. Their product yields the deposition probability and is used to calculate the deposition rate coefficient, k , of the entire (upscaled) porous media, assuming first-order kinetics [42,27,43].

Classic filtration models predict (i) retained colloid concentrations (depth profiles) that decrease exponentially with distance from the source and (ii) breakthrough-elution concentration histories that are near Gaussian. Nonetheless, observations of non-exponential depth profile shapes (e.g., hyper-exponential, uniform, non-monotonic) and heavy-tailed breakthrough curves are ubiquitous [18–25], suggesting that transport dynamics cannot be properly captured by a simple first-order k . Recent advancements in modeling efforts that can account for such anomalies have comprised pore-scale kinetic theory upscaling [44], probability distributions of fluid velocities and deposition rates [45], as well as the use of multiple rates for attachment [46,47], and explicit modeling of particle residence times at the near-surface fluid domain [6,17,48]. Because models of this sort are based on inferences, further efforts are needed to, on the one hand, provide experimental observations of particle spatial positioning to validate the underlying assumptions, on the other hand, corroborate the significance of the modeled mechanisms under varied conditions.

The overarching objective of this work is to understand the multi-scale processes driving colloid transport and retention in *unfavorable* surface heterogeneous porous media. Specifically, we compare experiments and simulations of colloid transport and retention from the interface-, collector-, pore-, and up to the Darcy-scale (see Fig. 1)) to i) represent the variability of colloid-grain interactions under surface heterogeneity; ii) determine the mechanisms driving colloid retention at available pore-scale retention sites and; iii) predict anomalous depth profiles and breakthrough curves with a physics-based upscaling approach. To the authors' knowledge, this work presents for the first time the interrelation between experimental spatial positioning of transported colloidal particles in porous media and equivalent simulations from a mechanistic model at multiple scales.

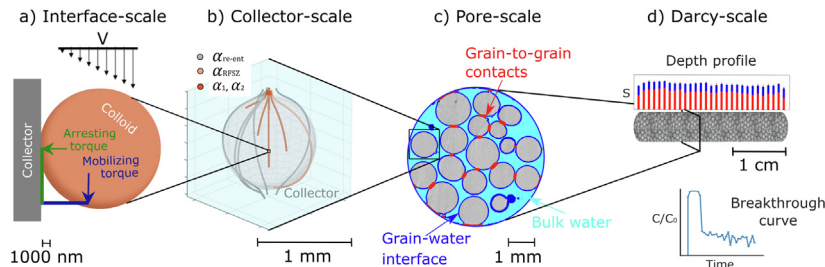


Fig. 1. Upscaling schematic for colloid transport in a porous medium. a) Velocity profile and the torques acting over a single colloid near the collector surface (modified from VanNess et al., (2019) [52]). b) Lagrangian colloid trajectories within a representative elementary volume, a single grain with flow, as color-coded by their retention mechanism. c) Pore-scale retention sites where colloids can accumulate (from Patiño et al., (2022) [51]). d) Column packed with collectors from which DP and BTC signals are recovered.

2. Materials and methods

A link between the mechanisms responsible for colloid retention in porous media (from model simulations) and their fate (from experimental observations) is drawn at relevant scales ranging from the interface (angstroms to nanometers), collector and pore (micrometers to millimeters), to the Darcy-scale (few centimeters to meters) [41,49]. We consider the pore-scale as an ensemble of collector grains which differs from the collector-scale because it contains multiple grain-water interfaces and grain-to-grain contacts [50]. Simulations are performed with the mechanistic model Parti-Suite (PS) (<https://wpjohnsongroup.utah.edu/trajecoryCodes.html>). This model upscales interfacial interactions based on xDLVO, computes attachment efficiencies from Lagrangian colloid trajectories in a Happel-sphere geometry, and estimates macroscopic transport behavior as detailed depth profiles (DP) and breakthrough curves (BTC) from deposition rates determined at smaller scales. Input parameters for simulations were specified to be consistent with the experimental setup. Experiments from a silver colloid slug transported in a saturated glass bead-packed column (a model porous medium) that was subsequently imaged at high-resolution by X-ray micro-computed tomography (μ -CT) from Patiño et al. (2022), [51] are used for ground-truth comparison. Briefly, the available experimental data include: the mean-average ζ -potential of each material, pore-scale spatial distributions of retained colloids, and DPs of retained particles along the entire column length. Fig. 1 illustrates the workflow at different spatial scales.

2.1. Interface-scale: interaction energy profiles

Energy profiles of interaction between the silver colloids with surface roughness and glass beads with chemical microsites were estimated with the xDLVO module of PS [25]. The system represented is that of silver colloids interacting with glass beads immersed in water in the presence of surface heterogeneity. Considered interactions include van der Waals (V_{VDW}), electric double-layer (V_{EDL}), steric (V_{ST}), and Lewis acid-base interactions (V_{AB}) [53–55,43,56,57]. The analytical expressions for the various interactions (in sphere-sphere geometry) are provided in equations S1 to S4. The effective contact area over which a colloid and the grain interact is here referred to as the zone of interaction (ZOI). Its size, $R_{ZOI} = 2\sqrt{\kappa^{-1}r_p}$, is controlled by the Debye length of the solution κ^{-1} and the particle radius r_p [37]. The most unfavorable conditions for colloid-grain interactions take place when the entire ZOI falls outside the grain chemical heterodomains. Conversely, the most favorable conditions for colloid-grain interactions occur when the ZOI completely overlaps with a heterodomain region. All colloid-grain interactions are contained within these two extreme scenarios.

Hollow glass microspheres coated in a layer of silver (118 nm thick) were used as the colloidal particles for transport experiments (Microsphere Technology, Limerick, IE) with an average colloid radius, r_p , of 7.0×10^{-6} m. Similar colloids have been previously used to study biofilm distribution in porous media [58], and colloid retention at grain-to-grain contacts with μ -CT [22]. The colloids chosen for this study are larger than typical engineered silver colloids found in consumer products, but represent an idealized version of this kind of emerging groundwater contaminants [9,11]. The silver colloids were suspended in MilliQ water to achieve a concentration of 20 g L^{-1} , and used in experiments within 10 h. Borosilicate glass beads of 1.0×10^{-3} m mean diameter were used as the model porous medium (Sigma-Aldrich). To achieve $10 \mu\text{m}$ resolution μ -CT images, the packed bed was narrow (with ~ 5 grains in the transversal direction), but long (spanning more than 30 grain in the longitudinal direction). The measured average ζ -potential of the colloids and grains is considerably negative (-50 and -65 mV, respectively) [51]. It is expected that positively charged microsites are present on the grain surface, herein referred to as chemical heterodomains (CHD). In the absence of available direct measurements for CHD ζ -potential, we set its value to the opposite charge of the average grain surface (+65 mV). Rasmuson et al. (2019), [59] have reported that the primary control for attractive interactions between colloids and the collector is the presence of CHD, not the magnitude of their ζ -potential. Scanning electron microscopy (SEM) images of the silver microspheres suggest a mild level of surface roughness (refer to Fig. S1). Colloid asperities are therefore represented in the model as contiguous hemispheres with 20 nm height following the recommendations of Rasmuson et al. (2019) [59]. Table S1 summarizes all input parameters for the xDLVO module for PS.

2.2. Collector-scale & pore-scale: particle trajectories and retention sites

Simulated trajectories of colloids traveling in a Happel-sphere geometry (a representative elementary volume of a porous medium) were performed using the Traj-Hap module of PS. Briefly, Lagrangian trajectories are built as per the force-torque balance between colloid-CWI interactions and the flow field hydrodynamics (see Figs. 1a and b).

Trajectory results were then used to calculate the collector efficiency of the system, η , as the fraction of injected colloids that enter the near-surface pore water (separation distance between colloids and grain $< 200 \text{ nm}$ [39,48], approximately the thickness of the hydrodynamic boundary layer).

From η , we determine the fate of colloids in the near-surface (as number fractions) by one of four outcomes: fast attachment, α_1 , slow attachment, α_2 , re-entrainment, α_{re-ent} , or retention at the rear-flow stagnation zone, α_{RFSZ} . These number fractions are subse-

quently used to estimate multi-rate coefficients in the advective-dispersive reactive model described in Eqs. (1) to (3). In the Happel sphere domain, fast attachment refers to the colloids that deposit on the surface of the grain at comparable residence times to those of colloids deposited under favorable conditions. Conversely, slow attachment accounts for the colloids deposited on the surface of the grain at longer residence times than those in favorable conditions. Re-entrainment represents the colloids that entered the near-surface and exited back into the bulk solution. Retention at the rear-flow stagnation zone (RFSZ), occurs when colloids are dragged along the grain surface without contacting it until they reach the RFSZ of the grain, where they may remain for extended periods of time. [25]. To account for suspension polydispersity, as was determined experimentally in earlier work [60], we conducted simulations for 5000 trajectories of singlets ($r_p = 7 \times 10^{-6} m$), triplets ($r_p = 1 \times 10^{-5} m$), and tenplet colloid aggregates ($r_p = 1.5 \times 10^{-5} m$). Aggregates are represented as equivalent spheres of a larger effective size, which the results show is sufficient for modeling this simple system. However, exploring the shape of colloids and their aggregates presents an important opportunity for future research. Chemical heterodomains of 500 nm radius were uniformly distributed onto the grain with a surface coverage of 2%. The size of the CHD and the surface coverage were estimated following the recommendations in Ron et al., (2019) [39]. Trajectories were generated for two particle densities, $\rho_p \in [1.00, 1.03] \text{ g/cm}^3$, given slight variations in the customized colloid production. Table S2 summarizes all input parameters for the collector-scale module for PS.

Experimentally-observed spatial distributions of colloids at the pore-scale were used to quantify the dominant locations where particles are retained. Briefly, the column was non-destructively imaged by μ -CT to obtain a detailed three-dimensional map of the porous medium and the spatial distribution of retained colloids within it. Image segmentation was used to first define the bulk phases: grains, water, and retained silver colloids. Then, a sequence of image operations (dilate and intersect) was applied to define regions of interest (ROIs) corresponding to specific retention sites, including grain-water interface (GWI), grain-to-grain (GG) contacts, and bulk water (refer to Fig. 1c). The ROIs belonging to the retained silver and each retention site were processed in pairs with the intersection operation to determine the spatial positioning of the silver colloids. The reader is referred to Patiño et al. [51] for greater details on image processing. Fig. S2 illustrates the workflow for μ -CT image processing. At this scale, comparisons are drawn between the proportion of colloids retained by different mechanisms in the model (the mechanistic fate) and their distribution by retention site in the experiments (the spatial positioning). Statistical similarities between the two are ascertained with t-test analyses of the paired proportions.

2.3. Darcy-scale: deposition profiles and breakthrough curves

Detailed DPs and BTCs for the system were simulated with the Upscale-Continuum module of PS. The one-dimensional advective-dispersive-reactive model is based on the following set of governing equations [61]:

$$\frac{\partial C}{\partial t} \theta_b = D \frac{\partial^2 C}{\partial x^2} \theta_b - v \frac{\partial C}{\partial x} \theta_b - \alpha_1 k_f C \theta_b - (1 - \alpha_1) k_{ns} C \theta_b \quad (1)$$

$$\frac{\partial C_{ns}}{\partial t} \theta_b = (1 - \alpha_1) k_{ns} C \theta_b - v_{ns} \frac{\partial C_{ns}}{\partial x} \theta_{ns} - k_{f2}^* C_{ns} \theta_{ns} \quad (2)$$

$$\frac{\partial S}{\partial t} \rho_b = \alpha_1 k_f C \theta_b + k_{f2}^* C_{ns} \theta_{ns} \quad (3)$$

Here, C is the concentration of colloids in suspension, t is time, θ_b is the volumetric water content of bulk fluid in the representative elementary volume, D is the hydrodynamic dispersion coefficient, which includes α_L (the longitudinal dispersivity calculated as a function of the colloid size), and D^* , the diffusion coefficient of the colloids (calculated with the Stokes-Einstein Equation) [62,63], x is the distance along the column depth, v is the advective pore velocity, α_1 and k_f are the fraction and particle deposition rate coefficient of fast-attaching colloids, and k_{ns} is the rate coefficient for net transfer to the near-surface. C_{ns} is the concentration of colloids in the near-surface, v_{ns} is the near-surface fluid velocity determined from the residence time of the slow-attaching colloids [6], θ_{ns} is the volumetric water content in the near-surface fluid in the representative elementary volume, and k_{f2}^* is the rate coefficient for attachment of near-surface colloids when the near-surface fluid domain is explicitly simulated. S is the concentration of retained colloids and ρ_b is the bulk density of the medium. Note that the total volumetric water content in the representative elementary volume is $\theta = \theta_b + \theta_{ns}$.

The various rate coefficients were obtained considering the porous medium as a series of grains of identical diameter d_c following the upscaling strategy in Johnson et al., [48,6]. Consequently, k_f , k_{ns} and k_{f2}^* were explicitly calculated as [61]:

$$k_f = -\frac{3(1 - \theta_b)^{1/3}}{2d_c} \ln(1 - \eta)v, \quad (4)$$

$$k_{ns} = -v^* \frac{N_c}{L} \ln(1 - \eta(\alpha_2 + \alpha_{RFSZ} \alpha_{trans-gg} + \alpha_{re-ent})), \quad (5)$$

$$k_{f2}^* = -2 \frac{v_{ns}}{\pi d_c} \ln(1 - \eta \alpha_2). \quad (6)$$

Here, v^* is the characteristic velocity for scaling particle transfer to near-surface pore water (geometric mean between v and v_{ns}), N_c/L is the number of grains per unit length, and $\alpha_{trans-gg}$ is the fraction of colloids that after reaching the RFSZ of one grain, translate into the near-surface of the downstream grain in the upscaling model [6]. Table S3 summarizes all input parameters for the Upscale-Continuum module of PS.

By parameterizing the model with the above listed rate coefficients and setting the initial and boundary conditions to those used in the experiments (see Table S4), we obtain the DPs and BTCs for each aggregate size tested (singlets, triples, tenplets). The DPs are obtained for the total mass of retained material in depth, and also differentiated by the mechanism responsible for retention. A second set of simulations was performed at a time three times longer than the experimental duration to assess the heavy tail of the BTC. The results of the individual aggregate size simulations were combined to produce a final DP and BTC of a homoaggregated polydispersed system. The assumptions made are that the deposition phenomena is additive across polydispersed suspensions and that colloid-colloid interactions are negligible.

Experimental data at the Darcy-scale is focused on the DPs, which are provided both as the total mass of retained material in depth and differentiated by the specific pore-scale retention-site where the colloids were found (CWI, GG). BTCs from experiments are not available for comparison. At this scale, a link is made between the colloid's mechanistic fate in depth (from simulations) and their spatial positioning (from experiments). The coefficient of determination R^2 was used to obtain a goodness-of-fit between simulated and experimental results.

3. Results and discussion

3.1. Interface-scale: colloid-grain Interactions

In this section, the interaction energy between negatively-charged silver colloids and a chemically heterogeneous collector grain (mean negatively-charged surface, covered with positively-charged microsites) is presented as a function of the separation distance. At the interface scale, colloid behavior is driven by stochastic electric double-layer interactions, which are non-unique in surface heterogeneous systems and span from very repulsive to very attractive.

3.1.1. Experiments

Zeta potential values for the silver suspensions and the glass beads measured with a ZetaPlus analyzer (Brookhaven Instruments Corp., Holtsville, NY) were found to be -50 and -65 mV, respectively [64]. These measurements were used in the xDLVO module of PS as the surface charge for colloids and collector grain to calculate all interaction energy profiles.

3.1.2. Simulations

Fig. 2 shows an area plot of the range of theoretical net energies of interaction for a colloid approaching the surface of a grain with chemical heterogeneity. We argue that this representation is more appropriate than a single interaction profile when CHDs are present. Previous publications have underlined the limitations of assuming mean-field behavior for colloid-grain interactions [37,31,39,40]. The local charge at play, and therefore the net interaction, vary as the ZOI samples different portions of the surface with CHDs as illustrated in Fig. 2.

The dashed line in the plot illustrates the repulsive limit in our system. That is, the interactions between a silver colloid with -50 mV surface charge and a region of the grain surface with a local charge of -65 mV. The repulsive energy barrier in this extreme case reaches values of $\mathcal{O}(10^3)$ kT , which suggests negligible colloid deposition. Conversely, the solid line illustrates the

attractive limit herein considered. This represents interactions between a silver colloid with -50 mV surface charge and a region of the grain surface with a local charge of $+65$ mV. All intermediate colloid-grain interactions in our system are contained within these limits, and depend on how much the ZOI overlaps with a CHD onto the grain surface. Altogether, the unique interactions a colloid experiences with the heterogeneous grain are stochastic and therefore require a modeling framework that can account for such variability. Representing chemical heterogeneities is not straightforward as there is not yet an established way for their measurement and characterization [37,6]. Nonetheless, representing a more comprehensive range of interfacial interactions in models is an improvement to mean-field approaches, which omit the occurrence of some attractive interactions between colloids and grains that promote deposition in *unfavorable* conditions [37].

The conditions here tested are representative of environmental conditions encountered in typical soils and aquifers. Various external parameters may influence the zeta-potential heterogeneity (e.g., solution chemistry composition, nature of the microsite, mineral makeup of the porous medium), which can impact the magnitude of the stochastic interactions between colloids and CHD. A big opportunity exists in systematically exploring this variability in future work, which can be modeled and upscaled with the approach herein presented.

3.2. Collector- & pore-scale: mechanistic fate & spatial positioning

In this section, we compare the simulated transport mechanisms that include re-entrainment (exited colloids), fast and slow attachment (attached colloids), and accumulation without attachment at the near-surface of the grains (non-arrested near-surface colloids) against the pore sites where colloids are observed experimentally, namely GWI and GG, and the number of colloids within the bulk water and eluted from the media. At the collector scale, colloid behavior is driven by force-torque balances between colloidal net attraction (from stochastic electric double-layer interactions) and near-solid surface hydrodynamics.

3.2.1. Simulations

The results from upscaling simulations (Fig. 3, left-hand side) indicate that of the injected colloids, $\sim 62\%$ are eluted or exited from the porous medium (grey bar), $\sim 38\%$ attached to the grain surface (orange bar), and a small fraction ($< 1\%$) persist in the *near-surface* of the collector grains without proper attachment (tan bar). The latter fraction accounts for the mass that remains in the near-surface for long enough to be dragged or rolled by the flow to RFSZs. The error bars for these data indicate one standard deviation. Additional simulations were also conducted to assess immobilization trends in the absence of CHDs, equivalent to a homogeneous grain of uniform charge (see Fig. S3). This approach predicts 99.99% of the mass exited, 0% attached, and 0.01% retained at the *near-surface* at the end of the experimental transport tests. The lack of attachment is attributed to a consistently larger mobilizing torque than the arresting torque everywhere along the surface of the grain under homogeneously unfavorable conditions. Although a substantial fraction of injected colloids arrives at the near-surface, an insurmountable repulsion restricts attachment altogether.

3.2.2. Experiments

The results from experimental observations of accumulated colloids by pore-scale retention site are shown in Fig. 3, right-hand side. Approximately 58% of the injected mass was associated with the *bulk water* at the end of the transport tests (cyan bar), which represents colloids found in the effluent breakthrough and in the pore water because they were not flushed out long enough to exit

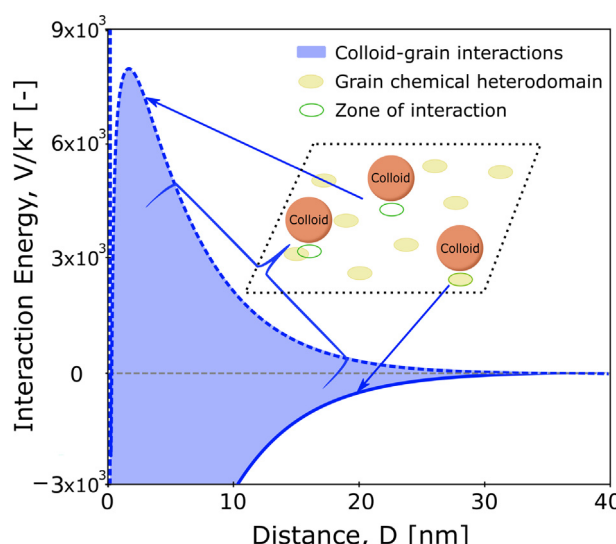


Fig. 2. Total interaction energy as a function of separation distance for a colloid approaching the surface of a grain with surface chemical heterogeneity. The dashed line shows the upper repulsive limit for the case where the ZOI between colloid and grain completely avoids heterodomains. The solid line shows the lower attractive limit for the case where the ZOI between colloid and grain falls completely within a heterodomain. Most interactions will fall between these two limits. The insert shows a schematic of three types of interactions possible.

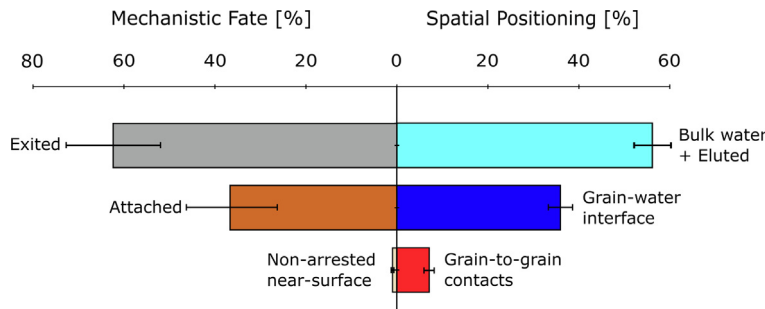


Fig. 3. Pore-scale mechanistic fate from simulations with chemical heterodomains vs. spatial positioning (colloid spatial distribution) from experiments.

the column. Approximately 35% of the colloids were found at the GWI (blue bar). That is, on the grain's surface, where it is expected that colloids are properly attached. Finally, around 10% of the injected mass was accumulated at GG contacts (red bar). These regions are defined by the intersection of multiple GWIs of neighboring grains and act as hydrodynamic traps for particles in regions of limited flow mobility [65–68]. The dominant spatial positioning in terms of particle retention is the GWI. However, it is important to note that the GG contacts are available in a lower proportion. Thus their contribution is still significant and should now be overlooked.

3.2.3. Quantitative comparison

Overall, the percentage of colloids subjected to the three mechanistic fates (simulations) and their corresponding spatial positioning (experimental observations) are in very close agreement (cf. symmetry in the left and right side of Fig. 3).

The percent of exited colloids in simulations is comparable to that of colloids found in the bulk water for experiments (gray and cyan bars, respectively). In this scenario, the colloids experience mobilizing torques that are greater than those required for arresting and are thereby able to exit the column entirely or avoid retention for the duration of the test. The percentage of attached colloids in simulations is comparable to that of experimental colloids found at the GWI (orange and blue bars, respectively). In this scenario, colloids experience a greater arresting torque than the mobilizing torque, likely because they encounter a grain CHD and the electrical-double layer interactions produce net attraction within the ZOI. This in turn allows a particle that is on the grain surface (the GWI) to become formally attached. Lastly, the percentage of simulated colloids at the near-surface is comparable to that of experimental colloids found at the GG contacts (tan and red bars, respectively). In this scenario, an approximate balance between mobilizing and arresting torques allows colloids to remain at the near-surface without physically contacting the grain, thereby sliding/rolling along the grain's surface until a RFSZ is reached where a neighboring grain is expected to be for a porous medium with structure. The small discrepancy in magnitude between this transport mechanism and its corresponding particle spatial positioning is likely due to colloids at GG contacts that have spent long enough times at such regions to become properly attached at CHDs in that vicinity. That is, some of the colloids that are attached are found at the GWI and within GG contacts.

To determine if the pairs of mechanistic fate and positional fate compared in Fig. 3 are statistically similar, two-tailed t-test were performed for each data pair. The results are presented in Table 1.

For all data pairs, $t_{\text{Stat}} < t_{\text{Critical}}$ values and $p\text{-values} > 0.05$, suggesting that the null hypothesis (the difference in group means is zero) cannot be rejected. That is, that the difference between the groups is not statistically significant.

Table 1

t-Test for pairs of mechanistic fate and positional fate samples assuming unequal variances.

Pairs	Exited & Bulk water + Eluted	Attached & Grain-water interface	Non-arrested near-surface & Grain-to-grain contacts
t Stat	0.500	0.077	6.065
t Critical two-tail	12.70	12.70	12.70
P($T \leq t$) two-tail	0.704	0.950	0.104

3.3. Darcy-scale: depth profiles & breakthrough curves

In this section, we compare the macroscopic transport behavior, with particular emphasis on the depth profiles, obtained from simulations and experiments. The simulated depth profile and BTC are based on the upscaling of the mechanistic fate outcomes, and are ultimately the result of considering CHD onto the surface of the collector grains. At the Darcy scale, colloid behavior is driven by advection, dispersion, and chemical non-equilibria that is parameterized in the form of force-torque imbalances that promote retention. Stacked bar charts are used in Fig. 4 to illustrate the proportion of colloids retained by mechanistic fate (in simulations) or by spatial positioning (in experiments) at each discretized depth. The error bars represent one standard deviation for each set of data.

3.3.1. Simulations

Simulated DPs (Fig. 4a) exhibit a non-exponential trend with depth (a sign of anomalous transport), capturing ~40% of the injected mass. This is in close agreement with experimental mass balance proportions (refer to Table S4). Here, we find that retention by attachment occurs at all depths (orange stacks) and that a consistently small but significant amount of colloids are associated to the near-surface (tan stacks) at depths greater than one third the column's total depth.

Simulated BTCs of colloids eluted from media with (cyan solid line) and without (grey dashed line) CHDs are shown in Fig. 5. In the presence of CHDs, the concentration signal shows exponential tailing (another sign of anomalous transport) with ~63% of the injected mass being eluted (see Table S4). The tailing in the BTC accounts for 11% of long term elution. By contrast, in the absence of CHDs, simulations predict 99.97% of the mass eluted after ~2.5 PV. The tailing in the BTC accounts for less than 1% of long term mass eluted. The near complete elution of colloids from the column (i.e., extreme lack of retention) is inconsistent with experimental observations and calls attention to the importance of incorporating surface heterogeneity in modeling efforts. Together, non-exponential DP and heavy-tailed BTC reveal anomalous transport behavior with considerable attachment when surface hetero-

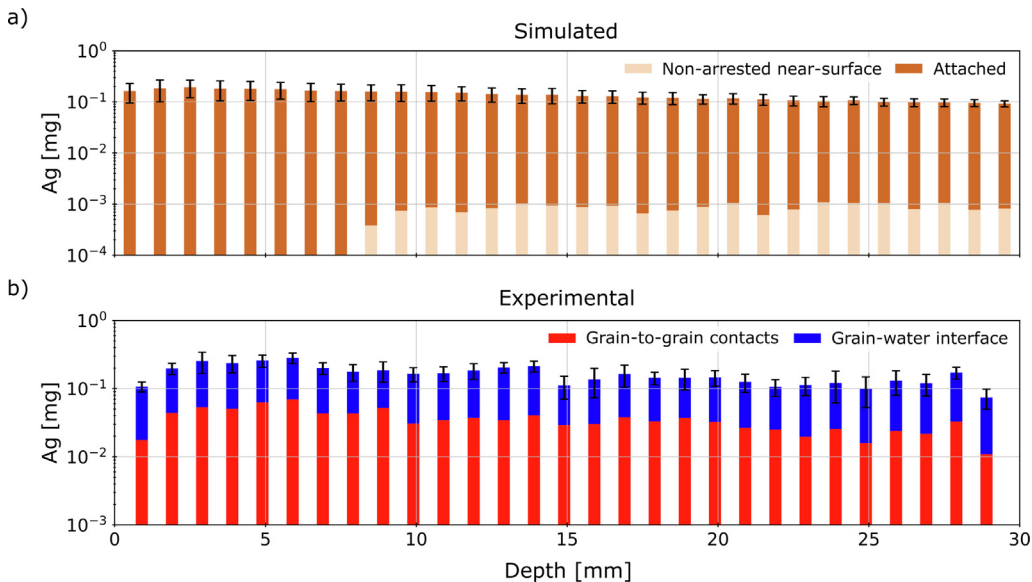


Fig. 4. Deposited colloid mass as a function of column depth. a) Model simulations further indicate the depth-dependent mechanistic fate (non-arrested near surface or attached). b) Experimental observations further indicate the depth-dependent spatial positioning (GWI or GG contacts). Error bars represent one standard deviation.

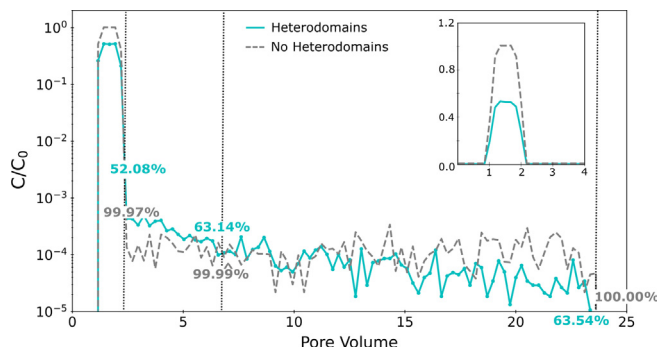


Fig. 5. BTCs of eluted colloids in the column. Solid and dashed lines correspond to simulations in the presence and absence of CHDs on the grain, respectively, in semi-log space. The first vertical line marks the main body of the BTC. The second vertical line marks the time when experiments were terminated. The insert shows the same data on linear-linear space. From these data it is evident that heterodomains cause significant retention with late time elution.

genetics are present. In this system, the anomalous signatures are attributed to broadly distributed colloid residence times. Importantly, our simulations show that heavy tailing results from re-entrainment of near-surface associated colloids.

3.3.2. Experiments

Experimental DPs (Fig. 4b) also exhibit a non-exponential (specifically, a non-monotonic) trend with depth, capturing ~43% of the injected mass. In this case, the retained mass is found primarily at the GWI (blue stacks) and secondarily at GG contacts (red stacks). Experimental BTCs of our system were very noisy with a low signal and were only used for computing mass balances.

3.3.3. Quantitative comparison

The coefficient of determination was used to assess goodness-of-fit between models and experiments in terms of the average mass deposited with depth (mean total DP). Here, we find that $R^2 = 0.997$ for the model considering CHD (Fig. 4) and $R^2 = 0.725$ for the model considering a chemically homogeneous grain surface (Fig. S4), appending evidence that our approach for modeling col-

loid retention in the presence of surface heterogeneity is very reasonable.

Although simulated and experimental DPs are consistent in terms of magnitude and shape of the total mass deposited, some apparent depth-dependent mismatches between mechanisms and pore-scale fate remain to be clarified. In particular, simulated DPs indicate that at shallow depths ($z \leq 8$ mm) particles are only attached, none are without contact at the near-surface, while experimental DPs show colloid retention at both the GWI and GG contacts at all depths. This is not inconsistent, considering that particles at shallow depths have spent the longest time in the domain. Therefore, it is conceivable that colloids that spend extended periods of time at the near-surface become funneled to RFZSs where they might find available CHDs to successfully attach. In a porous medium (grains with neighbors), the RFSZ of a grain would likely coincide with the near-surface of the grain downstream, forming a grain-to-grain contact. Evidence for this process has been shown in experiments and simulations documenting the PS software (<https://wpjohnsongroup.utah.edu/trajectoryCodes.html>), which supplements findings of the ubiquity of colloid retention at GGs (e.g., [51,22,23,69,70]). Thus, some colloids located at GG contacts may also be subject to attachment by the final time of the experiment. Finally, the small, but significant mass eluted in the heavy-tailed BTC suggests that even in a simple flow field, a broad distribution of colloid residence times can result in particles temporarily trapped in hydrodynamically stagnant zones from which they can re-enter into mobile pore regions and contribute to a low, but steady source of groundwater contamination.

4. Concluding remarks

Chemical surface heterogeneity in porous media has been associated with anomalous colloid transport behavior in environmental and engineering applications ranging from aquifer remediation to wastewater treatment [71,72]. However, for practical reasons it has been largely disregarded in modeling efforts [72]. The work presented sheds light on the mechanisms involved and the anomalous colloid transport expected in the presence of surface heterogeneity, and presents a modeling approach to account for the multiscale effects. Our model is novel in that it explicitly takes into

account diverse interactions between colloids and surface heterogeneities on the grain (interface-scale) and combines this with residence time spent in regions of low-flow (pore-scale) to accurately predict macroscopic anomalous transport behavior (Darcy-scale). From the proposed modeling approach, it is possible to estimate the late-time elution and distribution of permanently retained colloids in contaminated soils. Accurate mechanistic models are particularly important for colloid-size recalcitrant contaminants, which at low concentrations in environmental matrices still represent a considerable health threat [73,74].

In closing, the results of this study demonstrate that net attractive interactions between colloids and heterogeneous grains under unfavorable conditions are driven by electric double-layer interactions, which are stochastic and can produce attractive interactions despite the bulk average repulsion. This mechanism operates at the interface-scale and is further influenced by the system's hydrodynamics at the collector-scale, where immobilization of colloids is determined by the torque and force balance. At the Darcy-scale, an ensemble of collector grains, advection, and hydrodynamic dispersion become important for colloid transport and retention. Transport mechanisms, including fast and slow attachment, accumulation without contact at the near-surface, and reentrainment, play a role at the collector-scale, which was validated with pore-scale information on the spatial positioning of the colloids. Improving the predictive accuracy for colloid fate and transport in realistic porous media requires careful characterization and consideration of surface heterogeneities (chemical and physical), which we show should not be omitted in volume averaging approaches if accurate predictions are desired. Here, we provide a relatively parsimonious mechanistic model that upscales this important feature and demonstrates its physical correctness with rigorous comparisons against multiscale experimental observations.

Data availability

Data will be made available on request.

Declaration of Competing Interest

The authors declare that they have no known competing financial interests or personal relationships that could have appeared to influence the work reported in this paper.

Acknowledgement

This work was supported in part by the U.S. National Science Foundation (NSF) (EAR-1847689), the Engineering Research Center Program of NSF under Cooperative Agreement (EEC-1449501), the Donors of the American Chemical Society Petroleum Research Fund (59864-DNI9), Marie Curie Actions (FP7-PEOPLE-2012-SoilArchAg No. 302251), and the Miguel Velez Scholarship at the University of California.

Appendix A. Supplementary material

Supplementary data associated with this article can be found, in the online version, at <https://doi.org/10.1016/j.jcis.2023.03.005>.

References

- [1] C. Bianco, J.E. Patiño, T. Tosco, A. Tiraferri, R. Sethi, Controlled deposition of particles in porous media for effective aquifer nanoremediation, *Scient. Rep.* 7 (1) (2017) 12992.
- [2] D. Montalvo, R. Vanderschueren, A. Fritzsche, R.U. Meckenstock, E. Smolders, Efficient removal of arsenate from oxic contaminated water by colloidal humic acid-coated goethite: Batch and column experiments, *J. Clean. Prod.* 189 (2018) 510–518.
- [3] Z. Li, K. Greden, P.J. Alvarez, K.B. Gregory, G.V. Lowry, Adsorbed polymer and nom limits adhesion and toxicity of nano scale zerovalent iron to *e. coli*, *Environ. Sci. Technol.* 44 (9) (2010) 3462–3467.
- [4] C. Beer, R. Foldbjerg, Y. Hayashi, D.S. Sutherland, H. Autrup, Toxicity of silver nanoparticles—nanoparticle or silver ion?, *Toxicol Lett.* 208 (3) (2012) 286–292.
- [5] K. Mijnendonckx, N. Leys, J. Mahillon, S. Silver, R. Van Houdt, Antimicrobial silver: uses, toxicity and potential for resistance, *Biometals* 26 (4) (2013) 609–621.
- [6] W.P. Johnson, Quantitative linking of nanoscale interactions to continuum-scale nanoparticle and microplastic transport in environmental granular media, *Environ. Sci. Technol.* 54 (13) (2020) 8032–8042.
- [7] I. Sondi, B. Salopek-Sondi, Silver nanoparticles as antimicrobial agent: a case study on *e. coli* as a model for gram-negative bacteria, *J. Colloid Interface Sci.* 275 (1) (2004) 177–182.
- [8] J.-Y. Maillard, P. Hartemann, Silver as an antimicrobial: facts and gaps in knowledge, *Crit. Rev. Microbiol.* 39 (4) (2013) 373–383.
- [9] C. Zhang, Z. Hu, B. Deng, Silver nanoparticles in aquatic environments: Physiochemical behavior and antimicrobial mechanisms, *Water Resour.* 88 (2016) 403–427.
- [10] S. McGrath, A. Chang, A. Page, E. Witter, Land application of sewage sludge: scientific perspectives of heavy metal loading limits in europe and the united states, *Environ. Rev.* 2 (1) (1994) 108–118.
- [11] S.A. Blaser, M. Scheringer, M. MacLeod, K. Hungerbühler, Estimation of cumulative aquatic exposure and risk due to silver: contribution of nano-functionalized plastics and textiles, *Sci. Total Environ.* 390 (2–3) (2008) 396–409.
- [12] A.A. Keller, W. Vosti, H. Wang, A. Lazareva, Release of engineered nanomaterials from personal care products throughout their life cycle, *J. Nanopart. Resour.* 16 (7) (2014) 2489.
- [13] T.M. Benn, P. Westerhoff, Nanoparticle silver released into water from commercially available sock fabrics, *Environ. Sci. Technol.* 42 (11) (2008) 4133–4139.
- [14] R. Kaegi, A. Voegelin, B. Sinnet, S. Zuleeg, H. Hagendorfer, M. Burkhardt, H. Siegrist, Behavior of metallic silver nanoparticles in a pilot wastewater treatment plant, *Environ. Sci. Technol.* 45 (9) (2011) 3902–3908.
- [15] T. Benn, B. Cavanagh, K. Hristovski, J.D. Posner, P. Westerhoff, The release of nanosilver from consumer products used in the home, *J. Environ. Qual.* 39 (6) (2010) 1875–1882.
- [16] S.A. Bradford, V.L. Morales, W. Zhang, R.W. Harvey, A.I. Packman, A. Mohanram, C. Welty, Transport and fate of microbial pathogens in agricultural settings, *Crit. Rev. Environ. Sci. Technol.* 43 (8) (2013) 775–893.
- [17] I.L. Molnar, W.P. Johnson, J.I. Gerhard, C.S. Willson, D.M. O'Carroll, Predicting colloid transport through saturated porous media: A critical review, *Water Resour. Res.* 51 (9) (2015) 6804–6845.
- [18] S. Bradford, M. Bettahar, Straining, attachment, and detachment of cryptosporidium oocysts in saturated porous media, *J. Environ. Qual.* 34 (2) (2005) 469–478.
- [19] T. Tosco, M.P. Papini, C.C. Viggiani, R. Sethi, Nanoscale zerovalent iron particles for groundwater remediation: a review, *J. Clean. Prod.* 77 (2014) 10–21.
- [20] Z. Adamczyk, B. Siwek, M. Zembala, P. Belouschek, Kinetics of localized adsorption of colloid particles, *Adv. Colloid Interface Sci.* 48 (1994) 151–280.
- [21] C.-H. Ko, M. Elimelech, The shadow effect in colloid transport and deposition dynamics in granular porous media: measurements and mechanisms, *Environ. Sci. Technol.* 34 (17) (2000) 3681–3689.
- [22] X. Li, C.-L. Lin, J.D. Miller, W.P. Johnson, Pore-scale observation of microsphere deposition at grain-to-grain contacts over assemblage-scale porous media domains using x-ray microtomography, *Environ. Sci. Technol.* 40 (12) (2006) 3762–3768.
- [23] X. Li, C.-L. Lin, J.D. Miller, W.P. Johnson, Role of grain-to-grain contacts on profiles of retained colloids in porous media in the presence of an energy barrier to deposition, *Environ. Sci. Technol.* 40 (12) (2006) 3769–3774.
- [24] G. Malgaresi, B. Collins, P. Alvaro, P. Bedrikovetsky, Explaining non-monotonic retention profiles during flow of size-distributed colloids, *Chem. Eng. J.* 375 (2019) 121984.
- [25] W. Johnson, A. Rasmussen, E. Pazmiño, M. Hilpert, Why variant colloid transport behaviors emerge among identical individuals in porous media when colloid-surface repulsion exists, *Environ. Sci. Technol.* 52 (13) (2018) 7230–7239.
- [26] S. Xu, B. Gao, J.E. Sayers, Straining of colloidal particles in saturated porous media, *Water Resources Research* 42 (12).
- [27] N. Tufenki, M. Elimelech, Deviation from the classical colloid filtration theory in the presence of repulsive DLVO interactions, *Langmuir* 20 (25) (2004) 10818–10828.
- [28] B. Derjaguin, L. Landau, *Acta physicochim. urss.* J. of.
- [29] E.J.W. Verwey, J.T.G. Overbeek, K. Van Nes, *Theory of the stability of lyophobic colloids: the interaction of sol particles having an electric double layer*, Elsevier Publishing Company, 1948.
- [30] C.J. van Oss, *The extended DLVO theory*, Vol. 16, Elsevier, 2008.
- [31] E. Pazmino, J. Trauscht, B. Dame, W.P. Johnson, Power law size-distributed heterogeneity explains colloid retention on soda lime glass in the presence of energy barriers, *Langmuir* 30 (19) (2014) 5412–5421.
- [32] E. Pazmino, J. Trauscht, W.P. Johnson, Release of colloids from primary minimum contact under unfavorable conditions by perturbations in ionic strength and flow rate, *Environ. Sci. Technol.* 48 (16) (2014) 9227–9235.

[33] S. Torkzaban, S.A. Bradford, S.L. Walker, Resolving the coupled effects of hydrodynamics and dlvo forces on colloid attachment in porous media, *Langmuir* 23 (19) (2007) 9652–9660.

[34] S. Bhattacharjee, J.N. Ryan, M. Elimelech, Virus transport in physically and geochemically heterogeneous subsurface porous media, *J. Contam. Hydrol.* 57 (3–4) (2002) 161–187.

[35] C. Shen, B. Li, Y. Huang, Y. Jin, Kinetics of coupled primary-and secondary-minimum deposition of colloids under unfavorable chemical conditions, *Environ. Sci. Technol.* 41 (20) (2007) 6976–6982.

[36] W. Sang, V.L. Morales, W. Zhang, C.R. Stoof, B. Gao, A.L. Schatz, Y. Zhang, T.S. Steenhuis, Quantification of colloid retention and release by straining and energy minima in variably saturated porous media, *Environ. Sci. Technol.* 47 (15) (2013) 8256–8264.

[37] R. Duffadar, S. Kalasin, J.M. Davis, M.M. Santore, The impact of nanoscale chemical features on micron-scale adhesion: Crossover from heterogeneity-dominated to mean-field behavior, *J. Colloid Interface Sci.* 337 (2) (2009) 396–407.

[38] H. Ma, E. Pazmino, W.P. Johnson, Surface heterogeneity on hemispheres-in-cell model yields all experimentally-observed non-straining colloid retention mechanisms in porous media in the presence of energy barriers, *Langmuir* 27 (24) (2011) 14982–14994.

[39] C.A. Ron, K. VanNess, A. Rasmussen, W.P. Johnson, How nanoscale surface heterogeneity impacts transport of nano-to micro-particles on surfaces under unfavorable attachment conditions, *Environ. Sci.: Nano* 6 (6) (2019) 1921–1931.

[40] C.A. Ron, W.P. Johnson, Complementary colloid and collector nanoscale heterogeneity explains microparticle retention under unfavorable conditions, *Environ. Sci.: Nano* 7 (12) (2020) 4010–4021.

[41] J.N. Israelachvili, *Intermolecular and surface forces*, Academic press, 2011.

[42] K.-M. Yao, M.T. Habibian, C.R. O'Melia, Water and waste water filtration: concepts and applications, *Environmental science & technology* 5 (11) (1971) 1105–1112.

[43] M. Elimelech, J. Gregory, X. Jia, Particle deposition and aggregation: measurement, modelling and simulation, Butterworth-Heinemann, 2013.

[44] D. Fan, E. Chapman, A. Khan, F. Iacoviello, G. Mikutis, R. Pini, A. Striolo, Anomalous transport of colloids in heterogeneous porous media: A multi-scale statistical theory, *J. Colloid Interface Sci.* 617 (2022) 94–105.

[45] F. Miele, P. De Anna, M. Dentz, Stochastic model for filtration by porous materials, *Physical Review Fluids* 4 (9) (2019) 094101.

[46] S.A. Bradford, S. Torkzaban, F. Leij, J. Simunek, M.T. van Genuchten, Modeling the coupled effects of pore space geometry and velocity on colloid transport and retention, *Water Resources Research* 45 (2).

[47] N. Sun, N.-Z. Sun, M. Elimelech, J.N. Ryan, Sensitivity analysis and parameter identifiability for colloid transport in geochemically heterogeneous porous media, *Water Resour. Res.* 37 (2) (2001) 209–222.

[48] W.P. Johnson, M. Hilpert, Upscaling colloid transport and retention under unfavorable conditions: Linking mass transfer to pore and grain topology, *Water Resour. Res.* 49 (9) (2013) 5328–5341.

[49] H. Vereecken, R. Kasteel, J. Vanderborght, T. Harter, Upscaling hydraulic properties and soil water flow processes in heterogeneous soils: A review, *Vadose Zone Journal* 6 (1) (2007) 1–28.

[50] S.A. Bradford, S. Torkzaban, Colloid transport and retention in unsaturated porous media: A review of interface-, collector-, and pore-scale processes and models, *Vadose Zone Journal* 7 (2) (2008) 667–681.

[51] J.E. Patiño, F.J. Pérez-Reche, V.L. Morales, Retention site contribution towards silver particle immobilization in porous media, *Water Resour. Res.* (2022). e2021WR031807.

[52] K. VanNess, A. Rasmussen, C.A. Ron, W.P. Johnson, A unified force and torque balance for colloid transport: Predicting attachment and mobilization under favorable and unfavorable conditions, *Langmuir* 35 (27) (2019) 9061–9070.

[53] J. Gregory, Approximate expressions for retarded van der waals interaction, *Journal of colloid and interface science* 83 (1) (1981) 138–145.

[54] S. Lin, M.R. Wiesner, Paradox of stability of nanoparticles at very low ionic strength, *Langmuir* 28 (30) (2012) 11032–11041.

[55] A. Grabbe, Double layer interactions between silylated silica surfaces, *Langmuir* 9 (3) (1993) 797–801.

[56] H.-J. Butt, B. Cappella, M. Kappl, Force measurements with the atomic force microscope: Technique, interpretation and applications, *Surface science reports* 59 (1–6) (2005) 1–152.

[57] J.A. Wood, L. Rehmann, Geometric effects on non-dlvo forces: relevance for nanosystems, *Langmuir* 30 (16) (2014) 4623–4632.

[58] G.C. Iltis, R.T. Armstrong, D.P. Jansik, B.D. Wood, D. Wildenschild, Imaging biofilm architecture within porous media using synchrotron-based x-ray computed microtomography, *Water Resources Research* 47 (2).

[59] A. Rasmussen, K. VanNess, C.A. Ron, W.P. Johnson, Hydrodynamic versus surface interaction impacts of roughness in closing the gap between favorable and unfavorable colloid transport conditions, *Environmental Science & Technology* 53 (5) (2019) 2450–2459.

[60] A.J. Perez, J.E. Patino, M. Soos, V.L. Morales, Morphology of shear-induced colloidal aggregates in porous media: Consequences for transport, deposition, and re-entrainment, *Environmental science & technology* 54 (9) (2020) 5813–5821.

[61] W.P. Johnson, E.F. Pazmiño, *Colloid (Nano- and Micro-Particle) Transport and Surface Interaction in Groundwater*, Guelph, Ontario, Canada, 2022.

[62] C. Zheng, MT3D: A modular three-dimensional transport model for simulation of advection, dispersion and chemical reactions of contaminants in groundwater systems, SS Papadopoulos & Associates (1992).

[63] C.V. Chrysikopoulos, V.E. Katzourakis, Colloid particle size-dependent dispersivity, *Water Resour. Res.* 51 (6) (2015) 4668–4683.

[64] J.E. Patiño, T.L. Kuhl, V.L. Morales, Direct measurements of the forces between silver and mica in humic substance-rich solutions, *Environ. Sci. Technol.* 54 (23) (2020) 15076–15085.

[65] J.E. Santos, D. Xu, H. Jo, C.J. Landry, M. Prodanović, M.J. Pyrcz, Poreflow-net: A 3d convolutional neural network to predict fluid flow through porous media, *Adv. Water Resour.* 138 (2020) 103539.

[66] P. de Anna, B. Quaife, G. Biros, R. Juanes, Prediction of the low-velocity distribution from the pore structure in simple porous media, *Phys. Rev. Fluids* 2 (12) (2017) 124103.

[67] S.A. Bradford, S. Torkzaban, A. Wiegmann, Pore-scale simulations to determine the applied hydrodynamic torque and colloid immobilization, *Vadose Zone Journal* 10 (1) (2011) 252–261.

[68] W. Zhang, V.L. Morales, M.E. Cakmak, A.E. Salvucci, L.D. Geohring, A.G. Hay, J.-Y. Parlange, T.S. Steenhuis, Colloid transport and retention in unsaturated porous media: Effect of colloid input concentration, *Environ. Sci. Technol.* 44 (13) (2010) 4965–4972.

[69] W. Johnson, X. Li, G. Yal, Colloid retention in porous media: Mechanistic confirmation of wedging and retention in zones of flow stagnation, *Environ. Sci. Technol.* 41 (4) (2007) 1279–1287.

[70] M. Tong, W.P. Johnson, Excess colloid retention in porous media as a function of colloid size, fluid velocity, and grain angularity, *Environ. Sci. Technol.* 40 (24) (2006) 7725–7731.

[71] D. Bolster, K.R. Roche, V.L. Morales, Recent advances in anomalous transport models for predicting contaminants in natural groundwater systems, *Curr. Opin. Chem. Eng.* 26 (2019) 72–80.

[72] Z. Guo, R. Ma, Y. Zhang, C. Zheng, Contaminant transport in heterogeneous aquifers: A critical review of mechanisms and numerical methods of non-fickian dispersion, *Sci. China Earth Sci.* 64 (8) (2021) 1224–1241.

[73] A. Cortis, T. Harter, L. Hou, E.R. Atwill, A.I. Packman, P.G. Green, Transport of cryptosporidium parvum in porous media: Long-term elution experiments and continuous time random walk filtration modeling, *Water Resour. Res.* 42 (12).

[74] P.C. Okhuysen, C.L. Chappell, J.H. Crabb, C.R. Sterling, H.L. DuPont, Virulence of three distinct cryptosporidium parvum isolates for healthy adults, *J. Infect. Diseases* 180 (4) (1999) 1275–1281.